AD-A038 558 AIR FORCE WEAPONS LAB KIRTLAND AFB N MEX F/G 20/3
FUNDAMENTAL ERRORS ASSOCIATED WITH THE GROSS MODELING OF THE PH--ETC(U)
FEB 77 M I SANCER F29601-75-C-0067
UNCLASSIFIED AFWL-TR-76-297 NL

CONT

AFWL-TR-76-297

AFWL-TR-
76-297

FUNDAMENTAL ERRORS ASSOCIATED WITH THE GROSS MODELING OF THE PHYSICAL FEATURES OF METALLIC ENCLOSURES

February 1977

Final Report

Approved for public release; distribution unlimited.

This research was sponsored by the Defense Nuclear Agency under Subtask No. DB-001, "Weapon Effects Assessment."

Prepared for
Director
DEFENSE NUCLEAR AGENCY
Washington, DC 20305

AIR FORCE WEAPONS LABORATORY
Air Force Systems Command
Kirtland Air Force Base, NM 87117

AFWL-TR-76-297

This final report was prepared by the Air Force Weapons Laboratory, Kirtland Air Force Base, New Mexico, under Contract F29601-75-C-0067, Job Order 12090502. Captain Michael G. Harrison (ELP) was the Laboratory Project Officer-in-Charge.

When US Government drawings, specifications, or other data are used for any purpose other than a definitely related Government procurement operation, the Government thereby incurs no responsibility nor any obligation whatsoever, and the fact that the Government may have formulated, furnished, or in any way supplied the said drawings, specifications, or other data is not to be regarded by implication or otherwise as in any manner licensing the holder or any other person or corporation or conveying any rights or permission to manufacture, use, or sell any patented invention that may in any way be related thereto.

This report has been reviewed by the Information Office (OI) and is releasable to the National Technical Information Service (NTIS). At NTIS, it will be available to the general public, including foreign nations.

This technical report has been reviewed and is approved for publication.

Michael G. Harrison

MICHAEL G. HARRISON
Captain, USAF
Project Officer

FOR THE COMMANDER

Aaron B Loggins

AARON B. LOGGINS
Lt Colonel, USAF
Chief, Phenomenology/Technology Branch

James L Griggs Jr

JAMES L. GRIGGS, JR.
Colonel, USAF
Chief, Electronics Division

DO NOT RETURN THIS COPY. RETAIN OR DESTROY.

UNCLASSIFIED

SECURITY CLASSIFICATION OF THIS PAGE *(When Data Entered)*

REPORT DOCUMENTATION PAGE	READ INSTRUCTIONS BEFORE COMPLETING FORM
1. REPORT NUMBER: AFWL-TR-76-297	2. GOVT ACCESSION NO. / 3. RECIPIENT'S CATALOG NUMBER
4. TITLE *(and Subtitle)*: FUNDAMENTAL ERRORS ASSOCIATED WITH THE GROSS MODELING OF THE PHYSICAL FEATURES OF METALLIC ENCLOSURES.	5. TYPE OF REPORT & PERIOD COVERED: Final Report. / 6. PERFORMING ORG. REPORT NUMBER
7. AUTHOR(s): Maurice I. Sancer *	8. CONTRACT OR GRANT NUMBER(s): F29601-75-C-0067
9. PERFORMING ORGANIZATION NAME AND ADDRESS: Air Force Weapons Laboratory (ELP) Kirtland Air Force Base, NM 87117	10. PROGRAM ELEMENT, PROJECT, TASK AREA & WORK UNIT NUMBERS: 64747F/12090502; Subtask No. DB001
11. CONTROLLING OFFICE NAME AND ADDRESS: Director Defense Nuclear Agency Washington, D.C. 20305	12. REPORT DATE: Feb[redacted]1977 / 13. NUMBER OF PAGES: 40
14. MONITORING AGENCY NAME & ADDRESS *(if different from Controlling Office)*: Air Force Weapons Laboratory Kirtland Air Force Base, NM 87117	15. SECURITY CLASS. *(of this report)*: UNCLASSIFIED / 15a. DECLASSIFICATION/DOWNGRADING SCHEDULE

16. DISTRIBUTION STATEMENT *(of this Report)*

Approved for public release; distribution unlimited.

17. DISTRIBUTION STATEMENT *(of the abstract entered in Block 20, if different from Report)*

18. SUPPLEMENTARY NOTES

*Partially supported by an Air Force contract to him as an individual and partially as a consultant to Research and Development Associates supported by a contract with DNA.

19. KEY WORDS *(Continue on reverse side if necessary and identify by block number)*

Electromagnetic Fields and Waves
Aircraft Models
Circular Cylinders
Electromagnetic Pulse Interaction
Electromagnetic Pulse

20. ABSTRACT *(Continue on reverse side if necessary and identify by block number)*

It is demonstrated that for a significant band of low frequencies the current density induced on several objects predominantly has a magneto-static behavior. This result is shown to be in conflict with common modeling assumptions and it is subsequently interpreted to be of assistance for the determination of modeling requirements for future experimental and theoretical studies.

DD FORM 1 JAN 73 1473 EDITION OF 1 NOV 65 IS OBSOLETE

UNCLASSIFIED

SECURITY CLASSIFICATION OF THIS PAGE *(When Data Entered)*

013 150

18. SUPPLEMENTARY NOTES (Continued)

This research was sponsored by the Defense Nuclear Agency under Subtask No. DB-001, "Weapon Effects Assessment."

ACKNOWLEDGEMENTS

As indicated in the text, the technical material presented in this paper was developed over a period covering more than two years and is related to more than one contract. All of the contracts under which the technical work was accomplished were funded by the Air Force Weapons Laboratory. The organization, interpretation, and preparation of this work was performed at R & D Associates under Defense Nuclear Agency sponsorship.

In regard to the Air Force Weapons Laboratory sponsorship, I would like to give special thanks to Mike Harrison and Bill Prather who in addition to their sponsorship offered encouragement and appreciation of this work. I would also like to thank Carl Baum and Phil Castillo for their continuing support throughout the years.

Regarding the technical content, Ray Latham's contribution toward the understanding of the various phenomena played an essential part in the earlier presentation of some of this material, and his concepts provided insight concerning how to present some of the new results. Nasá Varvatsis was a co-author of the earlier work and made additional contributions to this work. Scott Siegel contributed to the technical content of this work in addition to performing all of the programming.

CONTENTS

ILLUSTRATIONS

SECTION 1
INTRODUCTION

This paper is basically an elaboration and an extension of some of our earlier work that has already been published [1]; however, there is an important difference between that work and this. Aside from the extension, the difference is that at this time we are fortunate to have high quality laboratory data available [2] for comparison with our calculations. We intend to take advantage of the degree of agreement of our calculations with these data to establish confidence in the credibility of our calculations for situations where no laboratory data are available.

Our claim is that an underlying assumption often used to justify the gross modeling of the physical features of metallic enclosures is in error. In order to clarify the relevance of the claim, the term "metallic enclosures" is meant to include structures such as aircraft, missiles, ships, and tanks. The specific assumption challenged is that if the wavelength of an incident monochromatic plane wave is long compared to the dimensions of a metallic structure, then the detailed features of the structure are not important for the subsequent modeling of the structure for EMP-related experiments or calculations. It is conjectured that the historical basis for this assumption is its validity for far zone calculations or measurements. The argument relating this frequency domain assumption to time domain EMP considerations is that the wavelengths in most of a representative EMP spectrum are long compared to many physical features of interest and we are not taking issue with this observation.

Our evidence to support our claim is based on external coupling analyses and measurements, and in presenting the

evidence we will focus our attention on the determination of surface current densities. The reason for focusing on densities is that it is these quantities that are a necessary part of the external coupling information required by commonly employed deliberate antenna and aperture analyses for the subsequent calculation of voltages and currents driving mission-critical subsystems contained within the enclosure.

SECTION 2
OUTLINE OF EVIDENCE AND ARGUMENTS

We intend to establish confidence that our finite circular cylinder MFIE code can give reliable information where no measurements are readily available to us. In order to do this, we

- compare our current density calculations with those measured in a laboratory experiment
- argue that our code should perform at least as well at lower frequencies corresponding to the bulk of the energy for a typical spectrum of an EMP.

We will then present current density results obtained by running our finite circular cylinder code for a range of low frequencies and show that an appropriate magnetostatic current density solution describes the dominant behavior of the current density for an extended range of frequencies. Next we will explain how this magnetostatic effect invalidates commonly employed external coupling approaches that assume a uniform circumferential distribution for the current density in order to determine this density simply by dividing a calculated bulk current by the circumference. In regard to this common assumption we will

- show that the density calculation becomes increasingly more inaccurate as the commonly stated validity conditions are increasingly better satisfied
- explain how the physical interpretation of a nonphysical situation is a likely candidate for the cause of the invalid assumption
- describe the impact on aircraft stick models and certain missile models.

The remaining material that will be presented is new in that it is what we referred to as the extension of Reference 1. We will present low frequency calculations using the MFIE approach for the current density induced on a finite cylinder having an elliptic cross-section. We then compare these finite elliptic cylinder results with an appropriate magnetostatic solution and again demonstrate that the dominant behavior is described by the magnetostatic solution for an extended range of frequencies. Using the magnetostatic solution, we obtain an analytic expression for the error that persists at low frequencies which is made by modeling the cross-section of an elliptic cylinder as a circle. The fact that there is any long wavelength error at all demonstrates that long wavelength arguments do not provide justification for gross modeling.

Finally, we present results based on symmetry arguments to qualitatively demonstrate the distribution of current density on a complex model of an aircraft at low frequencies. These results are equivalent to a magnetostatic solution, and consequently they differ from what would be obtained by a modeling that is insensitive to magnetostatic considerations.

SECTION 3
COMPARISON WITH EXPERIMENTAL DATA

The material presented in the first five figures in this paper contains material that was presented in two recent reports [2,3]. The curves in Figure 2 and the top portions of Figures 3, 4, and 5 are curves that were traced from Xerox copies of curves presented in those reports. The description of the experiment pertaining to the data presented in these figures is also redrawn based on a figure presented in Reference 2. The intent of this experiment is to simulate a monochromatic plane wave incident on a tube having a total length of 2h. By referring to Figure 1, we can see that the angle θ is defined so that 0° corresponds to the deep shadow region and 180° corresponds to direct illumination. The θ in Figures 3, 4, and 5 corresponds to this definition and z is the axial distance ranging from 0 at the ground plane to h at the top of the cylinder. The quantities $|K_z|$, $|K_\theta|$, and θ_z plotted in these figures are the magnitude of the axial component of the current density, magnitude of the transverse component of the current density, and the phase of the axial component of the current density. The same quantities calculated by our MFIE computer code for the current density induced by the same source on a flatly capped cylinder having the same length and diameter as the tube of the experiment are presented in the bottom half of Figures 3, 4, and 5. The scales of our calculations were adjusted to the scales of the experimental data by using three numbers, a multiplicative factor for each set of the magnitude comparisons and an additive factor for the set of phase comparisons. These three numbers were determined by forcing one point of the experimental data to match one point of our calculated data on only one curve of each of the three sets of curves. The reason we include Figure 2 in this paper

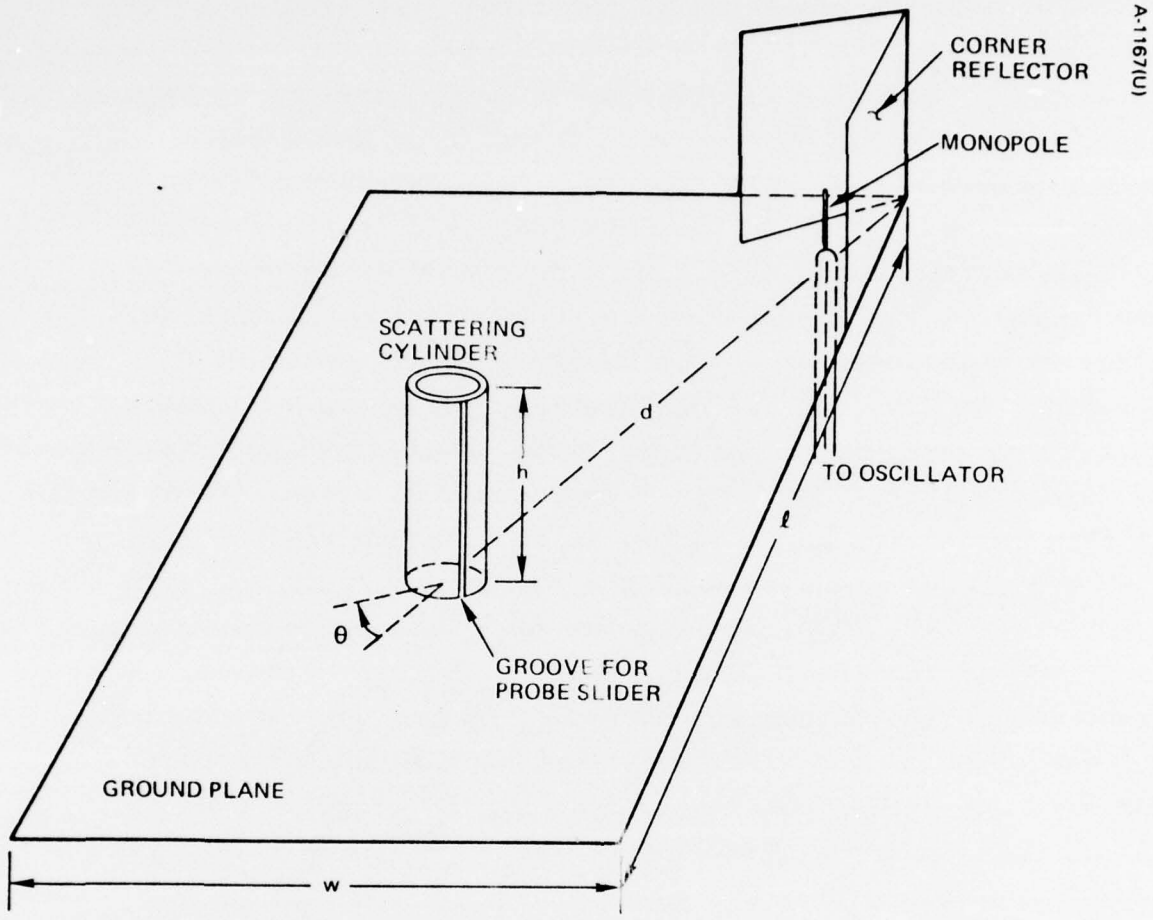

Figure 1. Schematic Diagram of Scattering Cylinder on Ground Plane

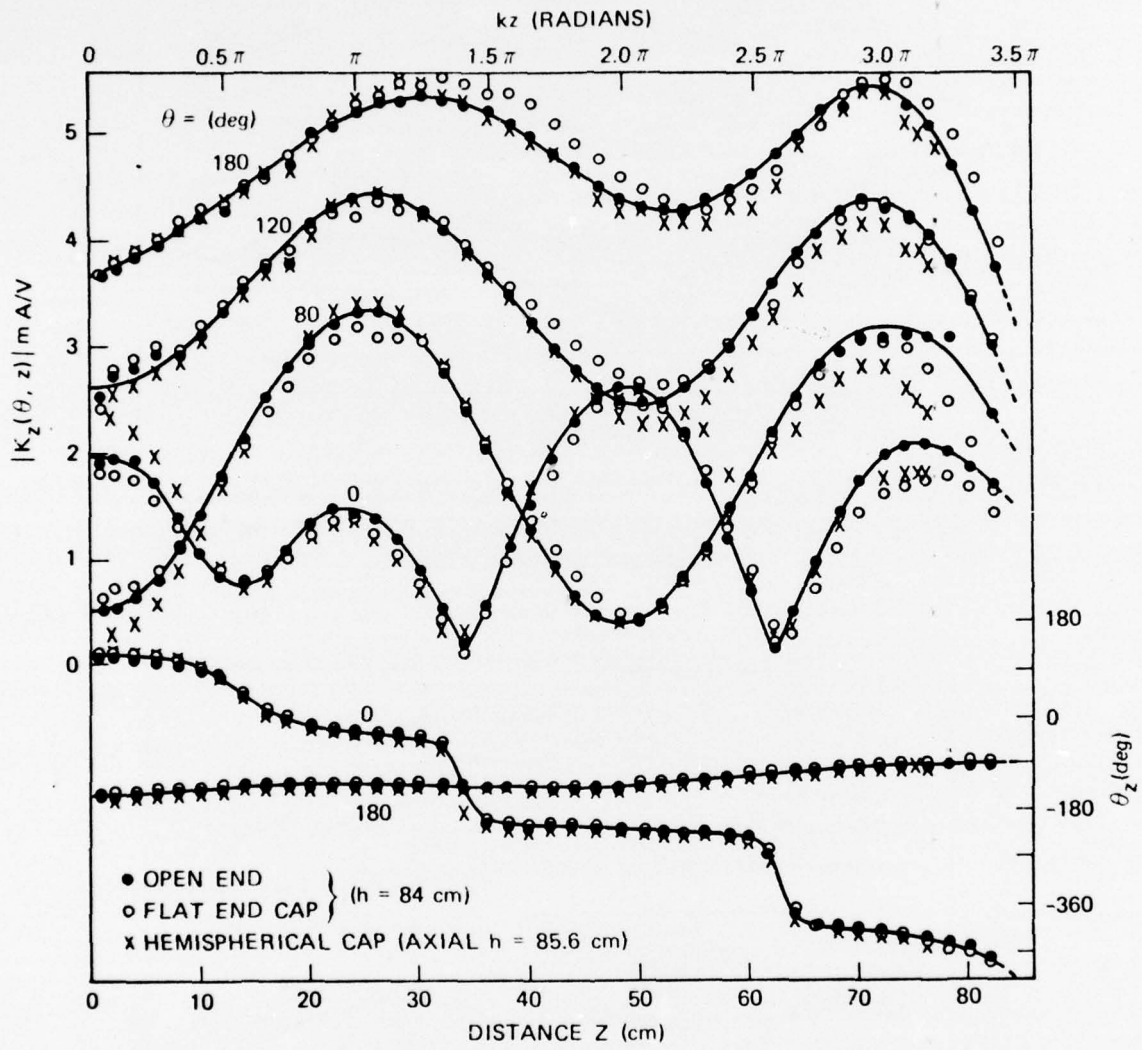

Figure 2. Measured Magnitude and Phase of Surface Density of Outside Axial Current on Tubular Cylinder with Open End, Flat and Hemispherical End Caps. E-Polarization.

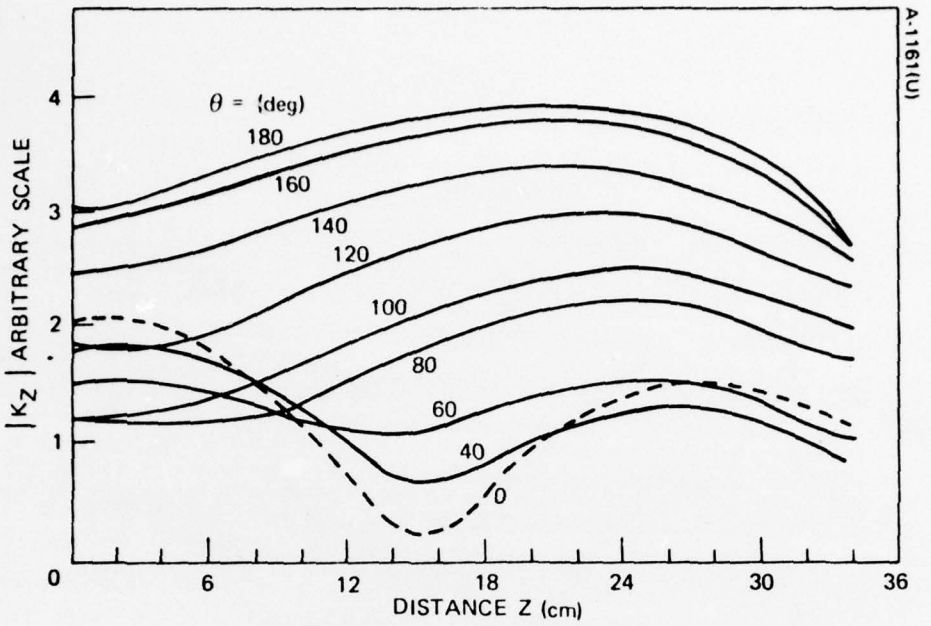

Figure 3a. Measured Amplitude of Axial Surface Density of Outside Current on Tubular Cylinder, E-Polarization (Large Outdoor Ground Screen)

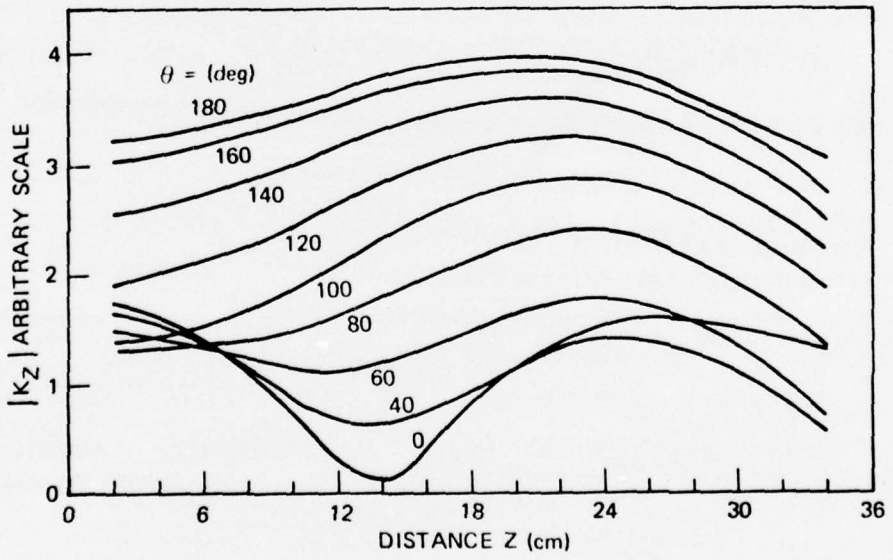

Figure 3b. Calculated Amplitude of Axial Surface Current Density on a Finite Circular Cylinder

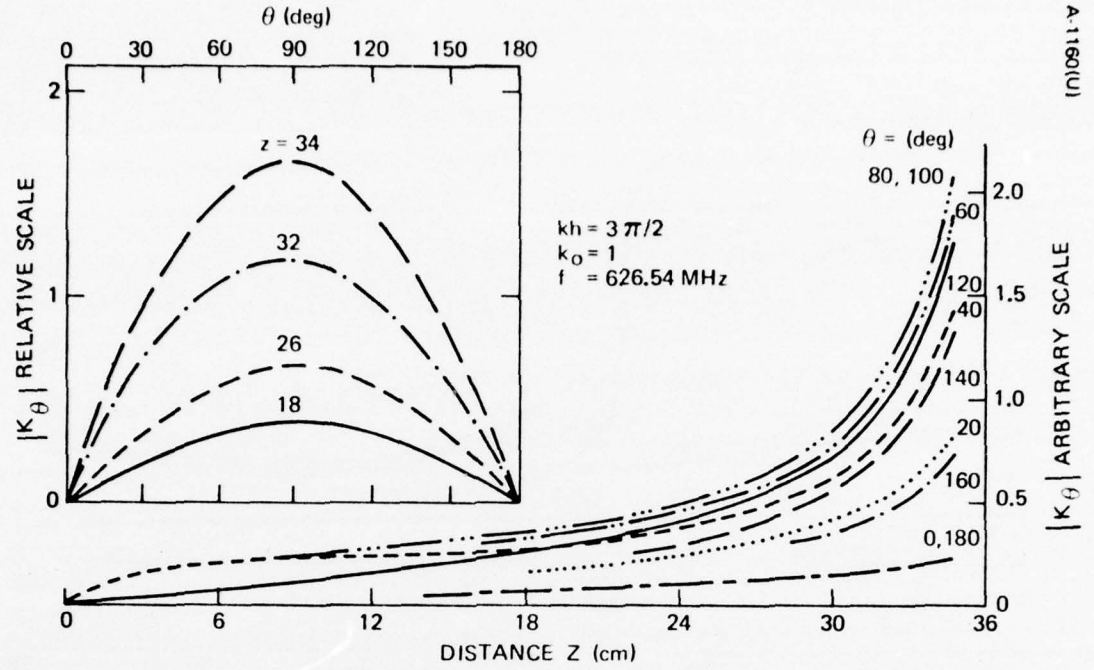

Figure 4a. Measured Amplitude of Surface Density of Transverse Current on Tubular Cylinder, E-Polarization; Normal Incidence (Large Outdoor Ground Screen)

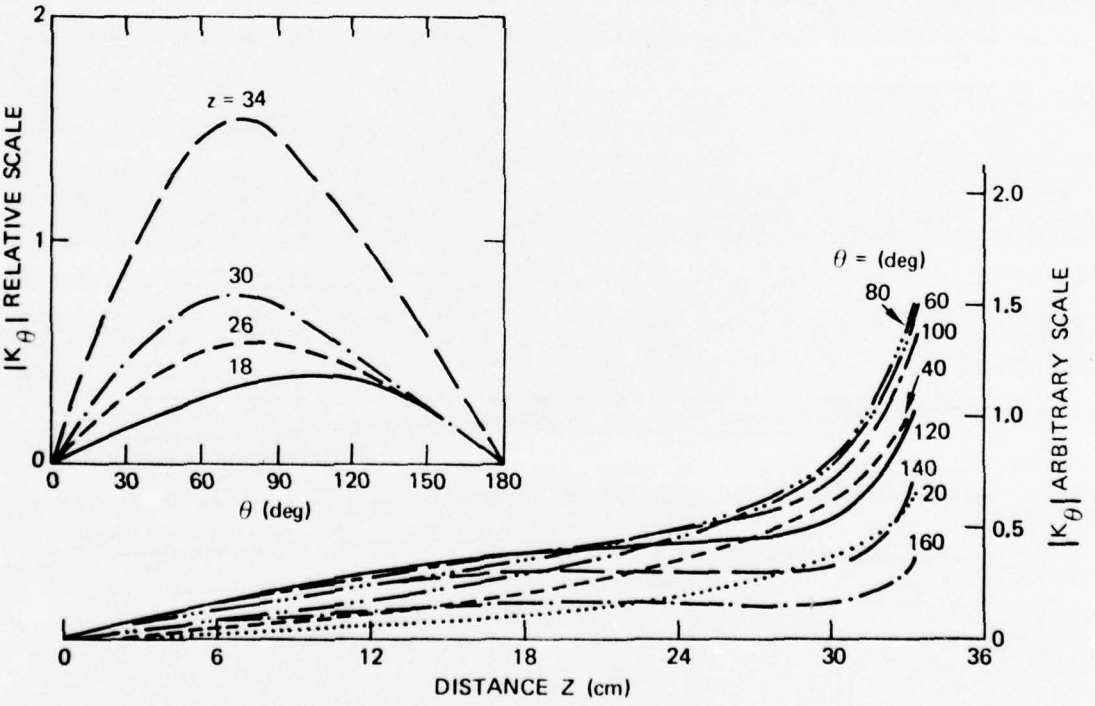

Figure 4b. Calculated Amplitude of Transverse Surface Current Density on a Finite Circular Cylinder

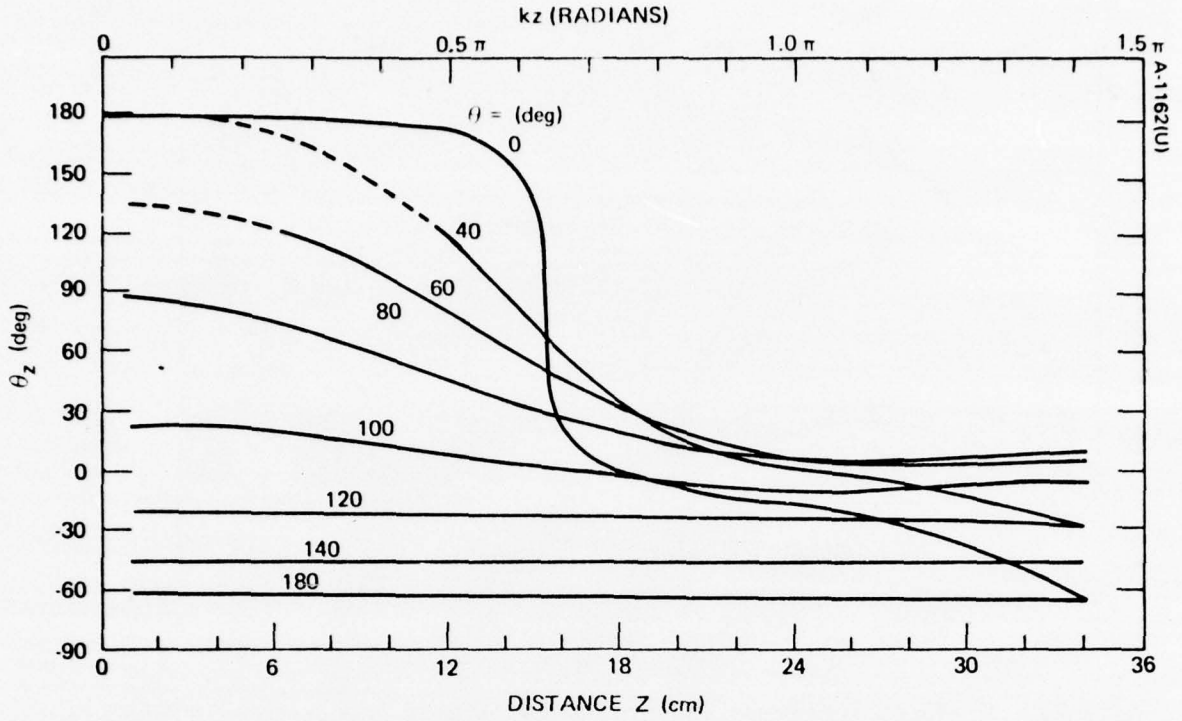

Figure 5a. Measured Phase of Axial Surface Density of Outside Current on Tubular Cylinder. Normalization: $-\phi_{obs}$ (Large Outdoor Ground Screen)

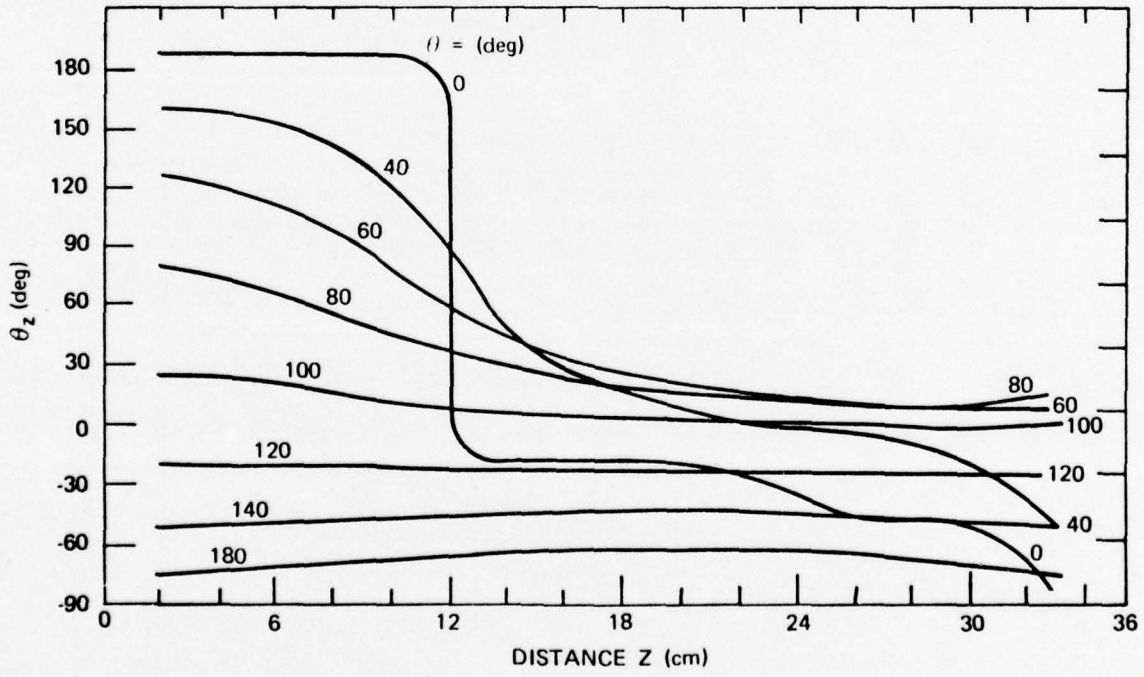

Figure 5b. Calculated Phase of Axial Surface Current Density on a Finite Circular Cylinder

is to show that there is only a minimal measured effect of capping the tube, thus justifying our comparison of the capped tube calculations to the uncapped measurements. It should be noted that our comparisons with the data were for h = 36 cm while the data in Figure 2 correspond to h = 84 cm.

Now it is necessary for us to discuss the frequency at which we made the comparison between our calculations and the experimental data. The normalized value kh = 1.5 π determines the frequency. First we note without scaling h to missile or aircraft size dimension that the comparison was made well beyond the primary resonance of the cylinder. Next we mention that if h is taken to be in the 10 to 20 m range, the frequency scales to the 20 to 10 MHz range. The main claim of this paper deals with low frequency behavior clearly below the frequency at which we made our comparison. In this regard, we claim that our MFIE approach can only perform better as the frequency is decreased. Without too much elaboration, the basic reason is that two types of zoning requirements had to be satisfied to obtain the agreement presented at kh = 1.5 π. One requirement is frequency independent and depends only on the geometry of the structure while the other is the usual frequency dependent requirement that no dimension of a zone should be greater than a tenth of a wavelength. The agreement at kh = 1.5 π insures that we have adequately determined the geometry requirement on the zoning and the frequency requirement becomes less restrictive as the frequency is decreased.

SECTION 4
LOW FREQUENCY FINITE CIRCULAR CYLINDER DATA

In Figure 6 we present the values of the axial component of current density $K_z(kh, z, \theta)$ obtained by running our code for the relatively low frequencies corresponding to kh ranging from 0.025 to 0.5. The real frequencies for these values of kh can readily be computed from the approximate formula

$$f \simeq 4.8(kh/d) \text{ MHz}$$

where d is the value of h expressed in tens of meters. The reason for expressing f in this form is that d will typically range between 1 and 2 since h will range between 10 and 20 m for typical aircraft and missile dimensions. The skin depth corresponding to this range of frequencies can readily be found in graphical form for different metals by referring to Reference 4. In addition to the skin depth being small for the band of frequencies corresponding to the data presented in Figure 6, nonplanar shielding studies as discussed in Reference 1 show that the frequency for which real metal can be considered perfectly conducting is even lower than what is indicated by having the skin depth being small compared to wall thickness. In summary, real metal used for aeronautical systems behaves as though it were perfectly conducting for the data presented in Figure 6.

The previous discussion regarding whether real metal can be considered perfectly conducting at these frequencies was presented in order to make the applicability of magnetostatics more palatable since it assumes a perfectly conducting boundary condition. Displayed in Figure 6 is an appropriate magnetostatic solution, the derivation of which appears in a later section of this paper. It is important to note that the magnetostatic solution describes either the dominant behavior or a significant part of the behavior for all the data displayed.

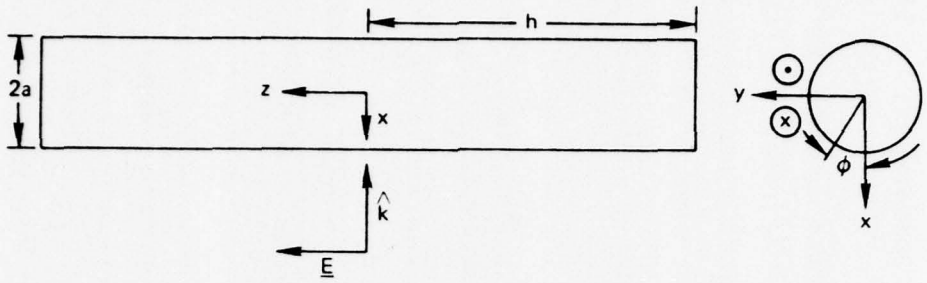

A-1163(U)

K_Z (kh, z, ϕ)

h/a = 10

z/h	kh	ϕ 15	45	75	105	135	165	K_Z (OLD) ALL ϕ
0.1	0.025		(1.41, - 0.08)			(-1.41, - 0.08)		(0+, - 0.08)
0.1	0.05		(1.41, - 0.16)			(-1.41, - 0.16)		(0+, - 0.16)
0.1	0.1		(1.41, - 0.32)			(-1.41, - 0.32)		(0+, - 0.32)
0.033	0.2	(1.92, - 0.67)	(1.41, - 0.65)	(0.52, - 0.64)	(-0.51, - 0.64)	(-1.41, - 0.65)	(-1.92, - 0.67)	(0+, - 0.65)
0.033	0.5	(1.96, - 1.93)	(1.46, - 1.88)	(0.56, - 1.84)	(-0.47, - 1.84)	(-1.37, - 1.88)	(-1.87, - 1.92)	(0.04, - 1.88)
MAGNETO-STATIC SOLUTION		1.93	1.41	0.52	-0.52	-1.41	-1.93	

$f \simeq 4.8$ (kh/d) MHz

$K_Z(\phi) = 2 \cos \phi$ (MAGNETOSTATIC SOLUTION)

NOTE: (ReK_z, ImK_z)

Figure 6. Low Frequency Calculated Amplitude of Axial Surface Current Density on a Finite Circular Cylinder

SECTION 5
CONSEQUENCES OF LOW FREQUENCY FINITE CIRCULAR CYLINDER DATA

One of the consequences is readily discussed by noting the column of data headed by K_z (old). These entries are values of the current density calculated by first integrating our current density with respect to ϕ, corresponding to integration with respect to circumferential arc length, in order to obtain a bulk current. Next we divide this bulk current by the circumference of the cylinder and denote the result as K_z (old). The reason for obtaining this quantity is that it corresponds to a common approach for obtaining this quantity. Specifically, it is often bulk current that is directly calculated and then current densities are assumed to be simply derivable by dividing the bulk current by a local circumference. It is assumed that this method of obtaining the current density becomes an increasingly better approximation as the wavelength increases relative to cross-section dimensions. By comparing K_z (old) to the actual values contained in the table, we see that it becomes an increasingly worse approximation as the wavelength is increased, i.e., kh decreases for a fixed h/a ratio. The fact that the approximation gets worse as the stated conditions for its validity become increasingly better satisfied indicates a fundamental error in interpreting the physics of the situation. Before completing this aspect of our presentation, we would like to clarify the fact that we are not claiming that the bulk current for fat cylinders has been incorrectly calculated. In fact, we obtain excellent agreement with the results presented in Reference 5 by integrating our current density. The claim is that a perfect knowledge of the bulk current, no matter how it is determined, cannot be used to obtain current density by dividing this quantity by the circumference.

The consequences of this erroneous assumption is that considerable effort has been devoted toward obtaining bulk current both computationally and experimentally when it is actually current density that is required. Until recently, the entire intent of aircraft stick models has been to obtain bulk current and then infer current density by dividing by the circumference. Regarding certain missile models, we were involved in calculating the bulk current induced on the various stages of Minuteman in flight. We then employed the assumption that we have demonstrated to be erroneous and divided the bulk current by the local circumference in the attempt to obtain the current density at various points of entry.

Returning to aircraft stick models, a recent modification has been to add a magnetostatic solution to the current density calculated in the old manner [6]. This has been shown to improve the calculation in that the results are in better agreement with laboratory measurements after the addition. The full implications of this modified approach deserve to be investigated and along these lines several issues are brought to mind by our experience. One issue is the determination of the conditions under which the total current density separates into the two separately calculable parts and another is how does one simply obtain a magnetostatic solution for a complex aircraft model.

SECTION 6

POSSIBLE EXPLANATION OF ORIGIN OF ERRONEOUS BULK CURRENT ASSUMPTION

In this section we will show how the physical interpretation of a nonphysical situation is a possible cause for the commonly employed erroneous assumptions. We will start with the standard solution for the current density induced on an infinitely long perfectly conducting cylinder; however, our interpretation of this equation is not the standard interpretation. For the geometry depicted below

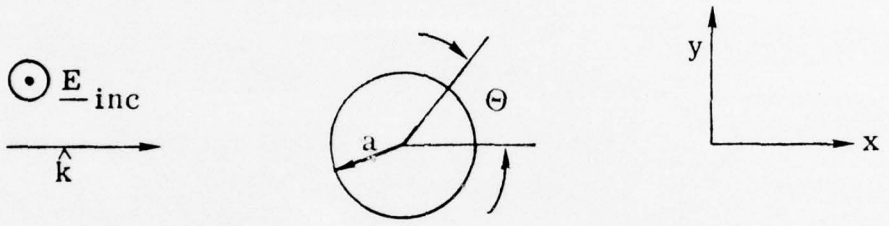

for

$$\underline{E}_{inc} = e^{ik_o x}\,\hat{z}$$

the current density induced on the cylinder K_z is given by

$$(\pi Z_o/2)K_z(\alpha,\theta) = \alpha^{-1}\left(\sum_{n=0}^{\infty} \frac{(i)^n a_n \cos n\theta}{H_n^{(1)}(\alpha)}\right) \equiv F(\alpha,\theta)$$

where $\alpha = k_o a = \pi \frac{2a}{\lambda}$, and $a_o = 1$, $a_n = 2 \quad n \geq 1$.

We now decompose $F(\alpha,\theta)$ into a part that is independent of θ and a remaining part that does depend on θ. That is

$$F(\alpha,\theta) = F_{ind}(\alpha) + R(\alpha,\theta)$$

where $F_{ind}(\alpha) = (\alpha H_o^{(1)}(\alpha))^{-1}$.

We now note that $F_{ind}(\alpha)$ approaches infinity as α approaches zero while $R(\alpha,\theta)$ is bounded for all α. The limit corresponding to α becoming increasingly small is the limit used to justify the approximation that the current density is uniformly distributed around the circumference of the cylinder, i.e., independent of θ. The following inequality based on the described behavior of $F_{ind}(\alpha)$ and $R(\alpha,\theta)$ is taken as the mathematical statement of the uniformity assumption

$$F_{ind}(\alpha) >> R(\alpha,\theta)$$

as α approaches zero. Our point is that this is a misleading and physically meaningless inequality when interpreted for cylinders of finite length. As a general rule it is dangerous to infer physical information concerning the relative largeness of a quantity going to infinity without investigating the reason for this quantity approaching infinity. In the situation presented here, by starting with the infinite cylinder solution it was never possible to determine the effect of relating the wavelength to the length of the cylinder. To provide a final argument to show that the relative largeness of $F_{ind}(\alpha)$ should not be used to infer finite length cylinder behavior, we note that the bulk current induced on the infinite cylinder is

$$I(\alpha) = a \int_0^{2\pi} K_z(\alpha,\theta)\, d\theta = (2a/\pi Z_o)\, F_{ind}(\alpha)$$

From this equation we see that the fact that $F_{ind}(\alpha)$ approaches infinity for small α causes $I(\alpha)$ to approach infinity for small α, while at the same time it is well known that $I(\alpha)$ for a cylinder of finite length approaches zero as α approaches zero.

SECTION 7
LOW FREQUENCY FINITE ELLIPTIC CYLINDER DATA

Figure 7 contains the values of the axial component of the induced current density $K_z(kh, h/12, \phi)$ obtained by running our code for the relatively low frequencies corresponding to kh ranging from 0.02 to 0.2. The real frequencies for these values of kh can be readily determined as described in Section 4, and the discussion concerning the applicability of perfectly conducting boundary conditions for real metal at these frequencies as presented in that section is also relevant for the data described in this section. Again, it is important to note that the magnetostatic solution describes either the dominant behavior or a significant part of the behavior for all the data displayed.

The derivation of the magnetostatic solution is explained in the next section, and the low frequency error factor is the ratio of the magnetostatic solution at $\phi = 0$ for $a \neq b$ divided by the evaluation for $a = b$. The significance of this low frequency error factor is also discussed in the next section.

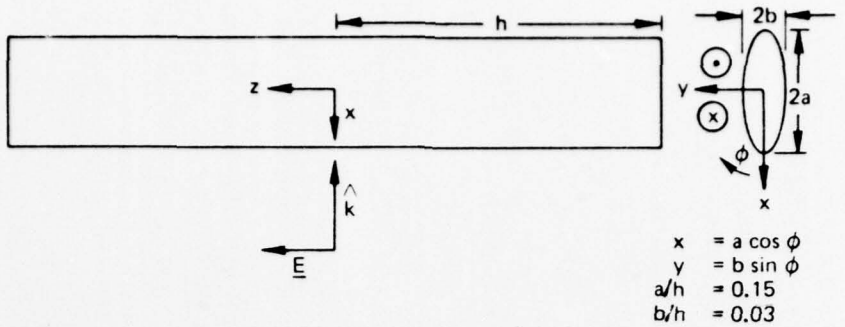

A-1164(U)

K_Z (kh, ϕ, z/h = 1/12)

kh \ ϕ	15	45	75	105	135	165
0.02	(3.49, - 0.19)	(1.19, - 0.09)	(0.33, - 0.06)	(-0.33, - 0.06)	(-1.19, - 0.09)	(-3.49, - 0.19)
0.04	(3.49, - 0.38)	(1.19, - 0.17)	(0.33, - 0.13)	(-0.33, - 0.13)	(-1.19, - 0.17)	(-3.49, - 0.38)
0.1	(3.49, - 0.95)	(1.19, - 0.43)	(0.33, - 0.32)	(-0.33, - 0.32)	(-1.19, - 0.43)	(-3.49, - 0.95)
0.2	(3.49, - 1.95)	(1.19, - 0.89)	(0.33, - 0.65)	(-0.33, - 0.65)	(-1.19, - 0.89)	(-3.48, - 1.95)
MANGETO-STATIC SOLUTION	3.59	1.18	0.32	-0.32	-1.18	-3.59

$f \simeq 4.8$ (kh/d)MHz

NOTE: (ReK_z, ImK_z)

$$K_Z(\phi) = \frac{(a + b)\cos\phi}{(a^2 \sin^2\phi + b^2 \cos^2\phi)^{1/2}} \quad \text{(MAGNETOSTATIC SOLUTION)}$$

LOW FREQUENCY ERROR FACTOR = (1 + a/b)/2

Figure 7. Low Frequency Calculated Amplitude of Axial Surface Current Density on a Finite Elliptic Cylinder

SECTION 8

APPROPRIATE MAGNETOSTATIC SOLUTIONS

In this section we will present a solution for the magnetostatic current density induced on an ellipsoid. By appropriately choosing the parameters describing the ellipsoid, we will obtain the magnetostatic solutions used to interpret the finite circular cylinder and finite elliptic cylinder results. The parameters of the ellipsoid, the orientation of the external magnetic field, and our coordinate system are displayed in Figure 8. We choose not to present the details of our derivation, as they will be presented shortly in a forthcoming AFWL technical report (7), and instead only present our results. The current density at points in the $z = 0$ plane only has a z-component which is

$$\underline{K}(\phi,z=0) = 2H_o b \cos\phi \, (2 - \alpha_o)^{-1} (a^2 \sin^2\phi + b^2 \cos^2\phi)^{-1/2} \hat{z}$$

where $x = a \cos\phi$

$y = b \sin\phi$

$\alpha_o = 2a(a + b)^{-1}(1 - \delta)$

$\delta = b(a - b)^{-1}(1 - (b/c)^2)^{-1/2}(E(\gamma,\beta) - (1 - (b/c)^2)^{1/2})$

and $E(\gamma,\beta)$ is an elliptic integral of the second kind requiring the further definitions

$$E(\gamma,\beta) = \int_o^\gamma (1 - \beta^2 \sin^2\tau)^{1/2} \, d\tau$$

where $\beta^2 = (1 - (a/c)^2)/(1 - (b/c)^2)$

$\gamma = \arccos(b/c)$

When $a = b$, then $\underline{K}(\phi,z=0)$ reduces to the spheriod solution given in Reference 1. In Reference 1, it was in effect stated that a quantity equivalent to our definition of δ was evaluated as 0.0203 for $a/c = b/c = 0.1$. This ratio of 0.1 was chosen

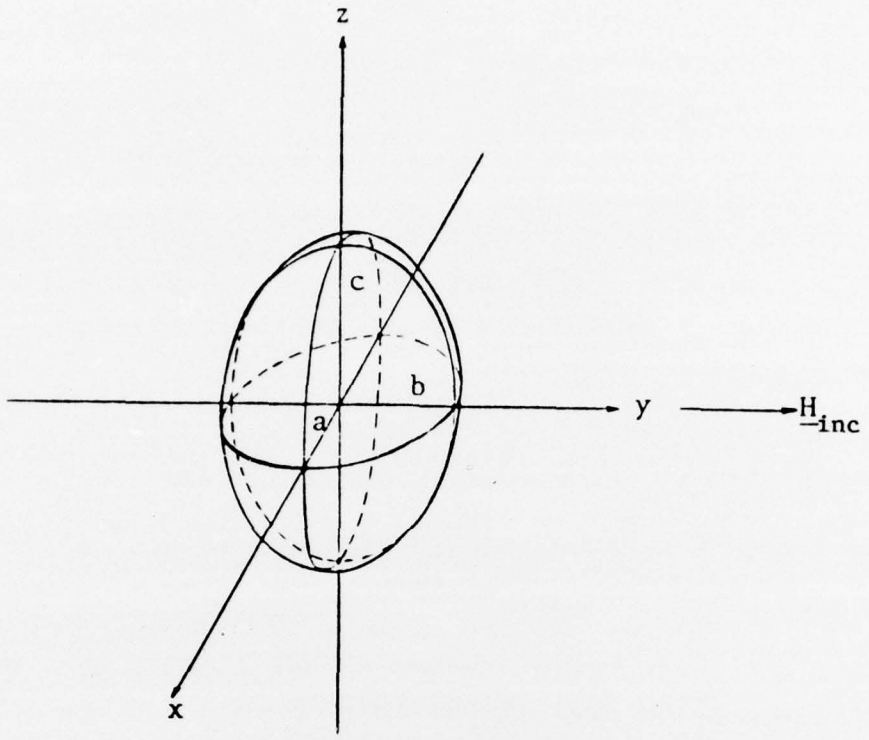

$$\frac{x^2}{a^2} + \frac{y^2}{b^2} + \frac{z^2}{c^2} = 1$$

Figure 8 . A perfectly conducting ellipsoid ($c \geq a \geq b$) in a magnetostatic field $\underline{H}_{inc} = H_o \hat{e}_y$.

to correspond to the length to diameter ratio of the circular cylinder for which we presented our data in Figure 6. The value of δ for a/c = 0.15 and b/c = 0.03 corresponding to the finite elliptic cylinder data presented in Figure 7 was also investigated. Due to the fact that we had limited tables of elliptic integrals and the fact that our intent is only to justify the approximation $\delta = 0$, we are content to say it is less than 0.01.

Finally we mention that δ does approach zero as c approaches infinity. The formula for $\delta = 0$ is

$$\underline{K}(\phi, z=0) = (a + b)\, H_o \cos\phi\, (a^2 \sin^2\phi + b^2 \cos^2\phi)^{-1/2}\, \hat{z} \tag{1}$$

and this solution is valid whether or not a and b are equal. For completeness, we exhibit the case where a = b, or

$$\underline{K}(\phi, z=0) = 2H_o \cos\phi\, \hat{z} \tag{2}$$

As shown in Figures 6 and 7, Equations 1 and 2 with the normalization $H_o = 1$ describe the dominant behavior of the current density induced in the vicinity of the center of a finite elliptic and circular cylinder for a band of frequencies.

Having established this, a significant point to be made by this paper is related to the fact that Equations 1 and 2 are not identical. The reason we make this statement is that if long wavelengths justified the gross modeling of physical features of structures, then one would not expect a significant difference of the current induced on a cylinder having an elliptic cross-section if the cross-section were modeled as a circle. A quick way to obtain a quantification of the error is to compare the value of the current density at $\phi = 0$. The resulting current density for a perfect measurement or calculation on a circular cylinder is 2 while if the real

cylinder had an elliptic cross-section the value should be 1 + a/b. Relating this result to the modeling of the wing of an aircraft where we might choose a/b = 8, then we see that there is an error factor of 9/2, where old long wavelength arguments would lead one to believe there should be no error at all. The full implications of this result go far beyond simple finite cylinders. New emphasis in deciding the amount of detail required for the modeling of physical features of metallic enclosures is warranted.

Finally, as a secondary issue and because of the fact that we have Equations 1 and 2 available for intrepretation, we are in a position to clarify a misconception regarding the magnetostatic solution for complex structures. It is that $2\hat{a}_z \cdot (\hat{n} \times \underline{H}_i)$ happens to equal the magnetostatic solution Equation 2; however, it is not a universal formula as can be seen from the fact that it does not equal Equation 1.

SECTION 9

QUALITATIVE LOW FREQUENCY CURRENT DENSITY DISTRIBUTION ON A COMPLEX AIRCRAFT MODEL

In describing this low frequency distribution we refer to Figure 9. The total extent to which we want to describe this distribution is contained in the two equations

$$\hat{t} \cdot \underline{K}(\underline{r}) = -\hat{t}' \cdot \underline{K}(\underline{r}') \tag{3}$$

$$\hat{s} \cdot \underline{K}(\underline{r}) = \hat{s}' \cdot \underline{K}(\underline{r}') \tag{4}$$

The derivation of these equations will appear in a forthcoming AFWL technical report (7). In order to explain these equations, it is necessary for us to still define $\hat{s}$, $\hat{t}$, $\hat{s}'$, and $\hat{t}'$ after noting that $\underline{K}(\underline{r})$ and $\underline{K}(\underline{r}')$ represent the surface current density evaluated at symmetric points with respect to the xy-plane. The vectors $\hat{s}$ and $\hat{s}'$ as well as $\hat{t}$ and $\hat{t}'$ are vectors tangent to the surface at the symmetric points $\underline{r}$ and $\underline{r}'$. In order for the relations (3) and (4) to be valid, these tangent vectors must have a more restrictive definition than the usual one which is that $(\hat{s}, \hat{t}, \hat{n})$ form an orthonormal set on the surface where $\hat{n}$ is the outward normal. In addition to this requirement, we will describe how $\hat{s}$ is defined so that $\hat{t}$ will then be determined by using the stated definitions of $\hat{n}$ and the orthonormality to give $\hat{t} = \hat{n} \times \hat{s}$. To describe $\hat{s}$ we imagine the body cut by planes parallel to the yz-plane and define $\hat{s}$ as the tangent vector to the curve formed by the intersection of these planar cuts with the body. In Figure 9 we display the curves and $\hat{s}$ vectors associated with two cuts through the body. In this figure we show several $\hat{t}$ vectors that are convenient to display as well as quantities $\underline{t}_{xz}$ and $\underline{s}_{xz}$ which are the xz projections of $\hat{t}$ and $\hat{s}$.

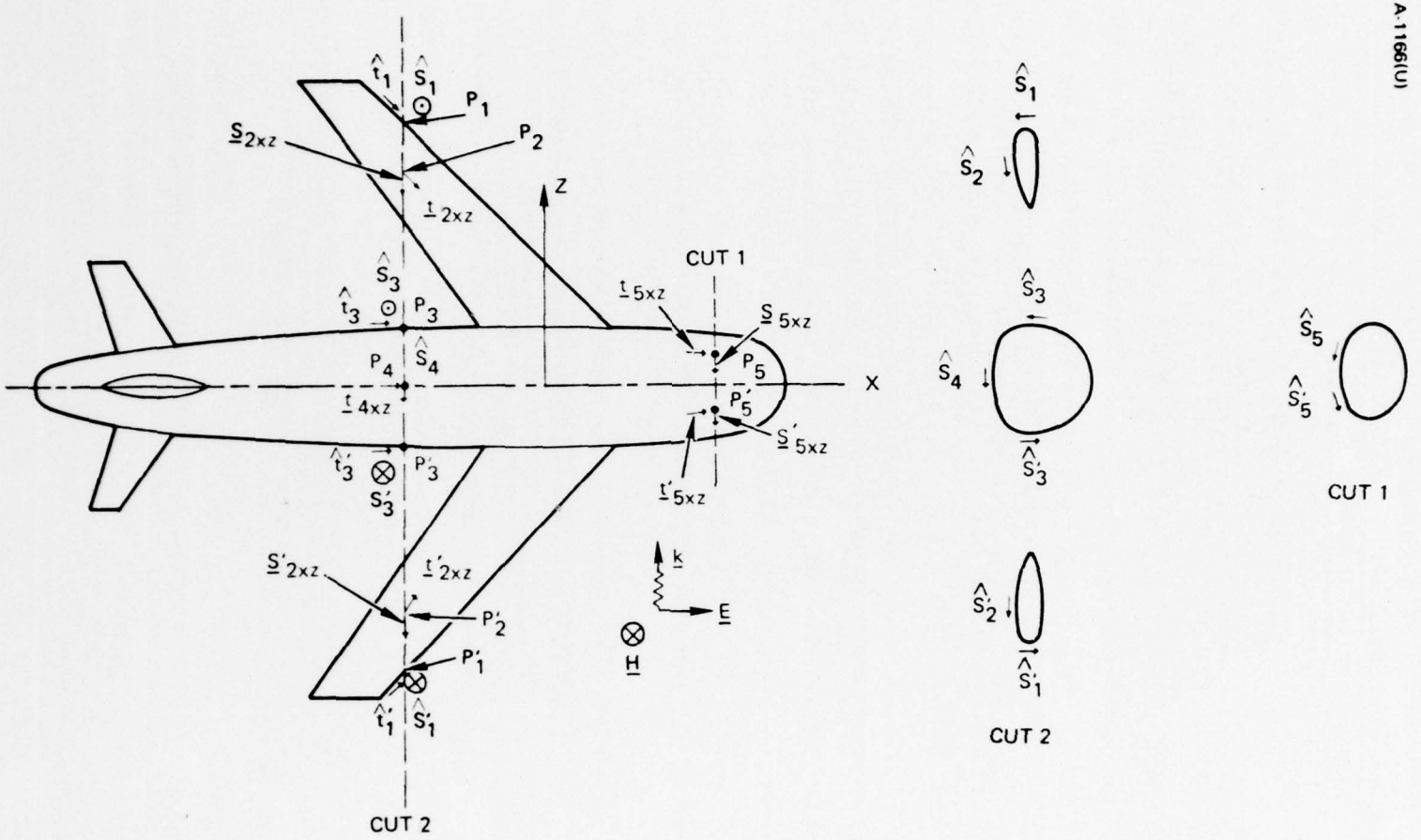

Figure 9. Description of $\hat{s}$ and $\hat{t}$ Vectors for an Aircraft

Now that the meaning of (3) and (4) has been explained, we would like to briefly describe the utility these equations can have in addition to their providing some qualitative insight concerning the induced current density distribution. We first note that (3) alone is sufficient to identify the error associated with current density calculations obtained by dividing a bulk current by a local circumference. This equation also provides enough information to draw the conclusion that $\hat{t} \cdot \underline{K}(r) = 0$ along the curve formed by the intersection of the xy-plane with the body.

Before concluding this section, we will present a brief outline concerning the derivation of (3) and (4). This derivation is a generalization of the derivation presented in Section 2 of Reference 1. It is possible to derive an integral equation for a quantity that when set equal to zero implies (3) and (4). It is argued that this quantity should be set equal to zero in the low frequency limit because the source term for the integral equation vanishes in this limit and the integral equation has a unique inverse. Finally, it can be shown that (3) and (4) are compatible with a magnetostatic solution for the aircraft model immersed in a static magnetic field oriented in the y direction.

SECTION 10
RECOMMENDATIONS

It has been demonstrated that for an extended band of low frequencies, the induced current density on several objects behaves predominantly like a magnetostatic solution. We conclude that the magnetostatic response of an object should be considered in determining low frequency modeling requirements for an external coupling analysis or measurement program. An appreciation concerning the significance of magnetostatics on determining modeling requirements can be obtained by noting the exact analogy between magnetostatics and irrotational and incompressible fluid flow around a rigid body. For a rigid perfectly conducting body, the velocity flow lines and the magnetic field lines in the vicinity of the body are identical.. If certain features of aircraft or missiles would have a significant effect on fluid flow, then they would have a significant effect on the current induced by an EMP. One should become concerned with modeling such features as missile tips and fins as well as aircraft features such as engines, wing cross sections, and extended junctions, particularly when the point of entry is in the proximity of these features.

Finally, it should be emphasized that magnetostatic considerations should only be part of a study to determine modeling requirements. The primary significance of magnetostatic related requirements is that they are much more severe than what has previously been thought justifiable as a result of considering long wavelength far zone scattering results.

In addition to the recommendations concerning modeling requirements, we would like to make the following recommendations:

- A thorough study should be initiated to determine the extent to which error and confidence requirements

for external coupling analysis should be diminished due to other uncertainties as well as excess hardening capabilities.

- In the interest of validation, the results of other measurement programs or analyses should be compared to the Harvard group's data and our MFIE code's calculations.

REFERENCES

1. M. I. Sancer, R. W. Latham, and A. D. Varvatsis, "Relationship Between Total Currents and Surface Current Densities Induced on Aircraft and Cylinders," EMP Interaction Notes, IN194, August 1974.

2. R. W. Burton, R. W. P. King, and D. Blejer, "Surface Currents and Charges on a Thick Conducting Tube in an E-Polarized Plane-Wave Field, II. Measurements," progress report on contract F29601-75-C-0019, Air Force Weapons Laboratory/ELPE, Kirtland Air Force Base, New Mexico, 1976.

3. R. W. P. King, "Surface Currents and Charges on a Thick Conducting Tube in an E-Polarized Plane-Wave Field, IV. Generalization to Cylinders of Various Lengths," progress report on contract F29601-75-C-0019, Air Force Weapons Laboratory/ELPE, Kirtland Air Force Base, New Mexico, 1976.

4. S. Ramo and J. R. Whinnery, Fields and Waves in Modern Radio, John Wiley and Sons, Inc., New York, p. 238, 1953.

5. R.W. Sassman, "The Current Induced on a Finite, Perfectly Conducting, Solid Cylinder in Free Space by an Electromagnetic Pulse," EMP Interaction Notes, IN11, July 1967.

6. C. D. Taylor, K. T. Chen, and T. T. Crow, "Electromagnetic Pulse Interaction with the EC-135 Aircraft," AFWL-TR-75-205, June 1976.

7. M. I. Sancer, S. Siegel, and A. D. Varvatsis, "Foundation of the Magnetic Field Integral Equation Code for the Calculation of Electromagnetic Pulse External Interaction with Aircraft," AFWL-TR-76-279, December 1976.

DISTRIBUTION LIST

1 Aeronautical Systems Division, ATTN: Capt David Guice/ENFTC, WPAFB, OH 45433

1 AFAPL/POD, ATTN: Duane G. Fox, SPAFB, OH 45433

1 RADC/EPER, ATTN: Richard B. Mack, Hanscom AFB, MA 01731

1 AFFDL/FGL, ATTN: G. A. DuBro, WPAFB OH, 45433

1 AFFDL/FES, ATTN: Capt Jerome T. Dijak, WPAFB, OH 45433

1 AFIT/ENE, ATTN: Lt William A. Davis, Electrical Engineering Dept, WPAFB, OH 45433

1 AFGL/OPR, ATTN: Lt John Little, Hanscom AFB, MA 01730

1 AFML/LG, ATTN: R. M. Neff, WPAFB, OH 45433

2 AFOSR/NP, ATTN: LtCol Gordon G. Wepfer, Physics Program/Bldg 410, Bolling AFB, Washington, DC 20332

1 AF/FTD, ATTN: ETET/Mr. Barry Ballard, WPAFB, OH 45433

1 AMSEL-TL-ENV, ATTN: Dr. H. A. Bomke, US Army Electronics Command, Fort Monmouth, NJ 07703

1 AMSEL-KL-TG, ATTN: William H. Wright, Jr., Fort Monmouth, NJ 07703

1 US Army Missiles Command, ATTN: H. Greene/AMSMI-RGP, Redstone, AL 35809

1 ASD/YH/EV, ATTN: Capt Clovis Hale, WPAFB, OH 45433

1 HQ USAF, ATTN: Maj Albert Bills/RDPE, Washington, DC 20331

1 DARPA, ATTN: Dr. Ernest F. Blase, 1400 Wilson Blvd, Rm 1039, Arlington, VA 22209

1 DNA, ATTN: Capt Doug Wilson/RAEV, Washington, DC 20305

1 HQ Electronic Systems Division, ATTN: Capt Larry West, YSEV/Stop 18, Hanscom AFB, MA 01730

1 CO, Harry Diamond Labs, ATTN: Dr. John Bombardt/AMXDO-EM, 2800 Powder Mill Road, Adelphi, MD 20783

1 Harvard University, ATTN: Prof. Ronald W. P. King, 9 Oxford Street, Cambridge, MA 02138

1 University of Illinois, Dept of EE, ATTN: Prof. Raj Mittra, Electromagnetics Lab, Urgana, IL 61801

1 NASA/IN-TEL32, ATTN: Carl Lennon, Kennedy Space Center, FL 32899

1 Kaman Sciences Corporation, ATTN: Dr. Walt Ware, POB 7463, Colorado Springs, CO 80907

1 University of Kentucky, Dept of EE, ATTN: L. Wilson Pearson, Lexington, KY 40506

1 Lawrence Radiation Laboratory, Livermore Division, ATTN: Dr. Andy Poggio, L156, POB 808, Livermore, CA 94551

1 Lawrence Berkeley Lab, University of California, ATTN: Dr. A. Sessler, Berkeley, CA 94720

1 Lightning Transients Research Institute, ATTN: J. D. Robb, 2531 W. Summer Street, St Paul, MN 55113

1 MIT Lincoln Lab, ATTN: Leona Loughlin/Tech Lib, 244 Wood Street, Lexington, MA 02191

1 Mission Research Corp, ATTN: Library, POB 8693, Albuquerque, NM 87108

1 University of Mississippi, Dept of EE, ATTN: Dr. C. Butler, Anderson Hall, University, MS 38677

1 Naval Surface Weapons Center, ATTN: Dr. Richard J. Wasneski, Code DF-12, Dahlgren, VA 22448

1 Naval Electronics Lab Center, ATTN: Dr. Jay Rockway/Code 2110, San Diego, CA 92152

1 US Naval Postgraduate School, ATTN: LtCol Robert W. Burton NC4(023A), Monterey, CA 93940

1 Naval Surface Weapons Center, ATTN: Louis F. Libelo/Phys Dept, White Oak, MD 20910

1 Naval Research Laboratory, ATTN: John D. Shipman, Washington, DC 20375

1 Rome Air Development Center, ATTN: Kenneth Siarkiewicz/RBCT, Griffiss AFB, NY 13441

1 Sandia Labs, ATTN: Robert Parker, Kirtland AFB, NM 87115

1 SAMSO/MNNH, ATTN: Maj Mike Baran/MNS-1, Norton AFB, CA 92409

Air Force Weapons Laboratory, Kirtland AFB, NM 87117 (Stop 53)

1 (HO/Dr. Minge)
1 (NT/Dr. Payton)
2 (SUL)
1 (DYT/Capt Wittwer)
1 (DYCS/Mr. Ady)
1 (DYS/Bill Baker)
1 (IN/John Elley)
2 (EL/Tech File)
1 (NT/John Darrah)
1 (NT/Dr. Baum)
1 (ELA/Dr. Castillo)
1 (ELA/Dr. Chen)
5 (ELP/Capt Harrison, Capt Hudson, B. Prather, Maj Covello, Maurice I. Sancer)

5 Project Officer, Capt Michael G. Harrison, AFWL/ELP, KAFB, NM 87117 (Stop 53)

1 HQ USAF (RDQSM/1D425), Washington, DC 20330

1 HQ USAF: AFTAC (TAP), Patrick AFB, FL 32925

1 AFSC (DLCAM), Andrews AFB, Wash, DC 20334

1 AUL (LDE), Maxwell AFB, AL 36112

1 AFIT (Tech Lib/Bldg 640/Area B), WPAFB, OH 45433

1 USAF, SCLO (Maj Pierson/Chief/LO), POB 348, Toronto, ON, Canada M5K 1K7

1 USAFA (DFSLB), CO 80840

1 USAFA (FJSRL/CC), CO 80840

1 AFFDL (DOO/Lib), WPAFB, OH 45433

1 AFGL, Hanscom AFB, MA 01730

1 RADC (Doc Lib), Griffiss AFB, NY 13441

1 AFRPL (DYSN), Edwards AFB, CA 93523

1 LLL (Lib/Bldg 50/Rm 134), Berkeley, CA 94720

1 Dir, LASL (Report Lib), POB 1663, Los Alamos, NM 87545

2 DDC (TCA), Cameron Station, Alexandria, VA 22314

1 Official Record Copy, AFWL/ELP (Capt Harrison, KAFB, NM 87117 (Stop 53)

Official Record Copy, AFWL/ELP (Capt Harrison, KAFB, NM 87117 (Stop 53)